GLOBAL BIOGEOCHEMICAL CYCLES, VOL. 14, NO. 4, PAGES 1267-1281, DECEMBER 2000

Sea-air CO_2 fluxes and carbon transport: A comparison of three ocean general circulation models

J. L. Sarmiento,[1] P. Monfray,[2] E. Maier-Reimer,[3] O. Aumont,[2] R. J. Murnane,[1,4] and J. C. Orr[2]

Abstract. Many estimates of the atmospheric carbon budget suggest that most of the sink for CO_2 produced by fossil fuel burning and cement production must be in the Northern Hemisphere. *Keeling et al.* [1989] hypothesized that this asymmetry could be explained instead by a northward preindustrial transport of ~1 Pg C y^{-1} in the atmosphere balanced by an equal and opposite southward transport in the ocean. We explore this hypothesis by examining the processes that determine the magnitude of the preindustrial interhemispheric flux of carbon in three ocean carbon models. This study is part of the first stage of the Ocean Carbon Model Intercomparison Project organized by International Geosphere Biosphere Programme Global Analysis, Interpretation, and Modelling Task Force. We find that the combination of interhemispheric heat transport (with its associated carbon transport), a finite gas exchange, and the biological pump, yield a carbon flux of only -0.12 to +0.04 Pg C y^{-1} across the equator (positive to the north). An important reason for the low carbon transport is the decoupling of the carbon flux from the interhemispheric heat transport due to the long sea-air equilibration time for surface CO_2. A possible additional influence on the interhemispheric exchange is oceanic transport of carbon from rivers.

1. Introduction

The emission of CO_2 to the atmosphere by fossil fuel burning and cement production averaged 5.4 ± 0.5 Pg C y^{-1} during the decade of the 1980s. Of this, only 3.2 ± 0.1 Pg C y^{-1} remained in the atmosphere. This implies a sink of ~2.2 ± 0.5 Pg C y^{-1} in the ocean and continental biosphere [*Schimel et al.*, 1995]. An essential problem in global carbon cycle research is the partitioning of this sink between the ocean and continental biosphere. Because of the interhemispheric asymmetry in the land and ocean distribution, much of the research on this issue has centered on the interhemispheric carbon budget.

A major constraint is that the observed north-south atmospheric CO_2 gradient of ~3 ppmv is lower than expected from fossil CO_2 emissions alone. Atmospheric general circulation models (GCMs) predict that the gradient due to fossil CO_2 emissions should be ~5-6 ppmv (assuming all of it remains in the atmosphere [*Tans et al.*, 1990; cf. also *Law et al.*, 1996]). The combined effect of terrestrial and oceanic sources and sinks, including land use changes such as tropical deforestation, must therefore be to give a larger fossil CO_2 sink in the Northern Hemisphere than in the Southern Hemisphere [e.g., *Ciais et al.*, 1995a; *Keeling et al.*, 1989; *Tans et al.*, 1990]. The problem of accounting for a large Northern Hemisphere sink is exacerbated by the fact that almost two-thirds of the oceanic sink of 2 ± 0.8 Pg C y^{-1} predicted by models is in the Southern Hemisphere due to its greater ocean area [*Sarmiento et al.*, 1992]. A further complication is the "rectification" effect, which is the net north-south CO_2 gradient at the surface that results from the interaction between a seasonally and diurnally varying atmospheric boundary layer and terrestrial biosphere with no net annual ecosystem production [*Denning et al.*, 1995; *Keeling et al.*, 1989]. Most models show a higher CO_2 in the Northern Hemisphere due to rectification [*Law et al.*, 1996], which enhances the need for a large Northern Hemisphere sink. However, the range in rectification obtained by the models is large, with one even showing lower CO_2 in the Northern Hemisphere.

An interhemispheric asymmetry in net fossil CO_2 sinks may be caused directly by anthropogenic perturbations such as deforestation/reforestation and oceanic uptake of anthropogenic carbon or indirectly by preindustrial asymmetries in natural processes. In the steady state carbon balance that we assume existed before the anthropogenic perturbation, one way to create such an asymmetry is by ocean transport. Over land, the steady state assumption requires a local balance of carbon fluxes between the atmosphere and the land. An exception to this is net continental CO_2 uptake by weathering reactions and net organic matter production and the associated river transport of carbon to the ocean [*Sarmiento and Sundquist*, 1992]. Within the ocean, it is possible for river input in one region to be connected by ocean transport to a region of release elsewhere.

Keeling et al. [1989] proposed that a preindustrial transport of carbon by the thermohaline circulation starting in the

[1] Atmospheric and Oceanic Sciences Program, Princeton University, Princeton, New Jersey.
[2] Laboratoire des Sciences du Climat et de l'Environnement, Commissariat à l'Energie Atomique, Centre National de la Recherche Scientifique and Institut Pierre Simon Laplace, Saclay, France.
[3] Max-Planck Institüt für Meteorologie, Hamburg, Germany.
[4] Now at Risk Prediction Initiative, Bermuda Biological Station for Research, Inc., Washington, DC.

Paper number 1999GB900062.
0886-6236/00/1999GB900062$12.00

North Atlantic is the major factor generating the interhemispheric asymmetry in anthropogenic carbon sinks. *Tans et al.* [1990], however, concluded that the asymmetry was due primarily to a large terrestrial sink in the boreal midlatitudes. The sink was attributed to direct anthropogenic perturbations and the indirect influence of anthropogenic perturbations on terrestrial biota (e.g., nitrogen and CO_2 fertilization). More recent analyses using $^{13}C/^{12}C$ and O_2/N_2 ratios measured during the 1990s have moderated these extreme points of view [*Ciais et al.*, 1995a; *Keeling et al.*, 1996]; but the problem is still not solved. A major concern in these studies is the difficulty of obtaining reliable long-term averages of the oceanic behavior. Analysis of atmospheric CO_2 and $^{13}CO_2$ measurements by *Francey et al.* [1995] and *Keeling et al.* [1995] suggest large interannual variability in ocean carbon sinks, although this is not supported by ocean modeling studies [*Le Quéré et al.*, 2000; *Winguth et al.*, 1994]. The approach we employ here is to use three-dimensional (3-D) ocean carbon cycle models (OCCMs) to estimate the long-term patterns of oceanic CO_2 sources and sinks, primarily for the preindustrial state.

A useful reference point for purposes of the present study is the estimate by *Keeling et al.* [1989] of a southward transport of ~1 Pg C y^{-1} within the ocean before the industrial revolution. All of this was postulated to occur in the Atlantic Ocean. Subsequent studies by *Broecker and Peng* [1992], *Keeling and Peng* [1995], and *Sarmiento et al.* [1995] have examined the role of the Atlantic thermohaline circulation in generating this interhemispheric transport. They estimated southward transports of 0.6, 0.4, and 0.2 Pg C y^{-1}, respectively. However, only recently has there been an attempt to explore the global carbon transport including the Indian and Pacific Oceans [*Murnane et al.*, 1999].

In this paper, we present global model results obtained as part of the first phase of the Ocean Carbon Model Intercomparison Project (OCMIP-1) organized by IGBP/GAIM. The goal of OCMIP is to improve our capacity to predict the evolution of oceanic carbon uptake and storage by comparison and evaluation of global OCCMs. Experiments dealing with the carbon system have been defined for both the natural cycle and anthropogenic perturbation. In addition, because ocean circulation is a major factor controlling the patterns of both the natural and anthropogenic carbon in the ocean, an early focus of OCMIP has been on the evaluation of the circulation by tracers such as $^{14}CO_2$ [*Orr*, 1999].

Two "gradient makers" act to create an inhomogeneous carbon distribution in the ocean. The "solubility pump" acts through sea-air gas exchange at the ocean surface where an atmosphere-ocean disequilibrium is created by a perturbation in the atmosphere, a heating or cooling of the ocean, or a change in ocean concentrations due to atmosphere-ocean water fluxes and river inflows. The "biological pump" removes inorganic carbon from surface layers during photosynthesis and transports this carbon down the water column before remineralization. It also reduces the surface alkalinity by removing $CaCO_3$, which is counterbalanced in the deep ocean by dissolution of $CaCO_3$. The cycling of nitrate in organic matter has an opposite but smaller effect on the alkalinity. Counteracting these two "gradient makers" is the oceanic circulation, which acts as a "gradient smoother," stirring and homogenizing the carbon distribution.

We present a set of simulations designed to identify separately the contribution of each of the important gradient-making processes to the present distribution of CO_2 sources and sinks. The approach we follow is that of *Sarmiento et al.* [1995] and *Murnane et al.* [1999], based on the insights of *Broecker and Peng* [1982] and the studies of *Volk and Hoffert* [1985], *Maier-Reimer and Hasselmann* [1987], and *Maier-Reimer* [1993]. The principal focus of our analysis is the influence of these processes on the interhemispheric transport of carbon and the sea-air flux.

2. Model Descriptions

Three groups participated in the full suite of OCMIP-1 results reported here: the Max Planck Institut für Meteorologie (MPI), Princeton University, and the Institut Pierre Simon Laplace (IPSL). Table 1 summarizes salient characteristics of the models and gives references. The models differ primarily in their horizontal and vertical resolution and numerical schemes. The IPSL model, in particular, has higher horizontal and vertical resolution than the Princeton or MPI models, and both the IPSL and MPI models have higher vertical resolution than the Princeton model. The MPI model uses upstream differencing, which has large numerical mixing in regions of high currents. The analyses of *Gerdes et al.* [1991] and *Maier-Reimer et al.* [1993] show that the mixing is relatively small throughout most of the ocean. The analysis of *Orr* [1999] shows that the centered differencing scheme used by the Princeton model gives sea-air fluxes that are virtually identical to the flux corrected transport multidimensional positive definite advection transport algorithm (MPDATA) method used in the IPSL model.

A further important difference in the models is that the IPSL model uses a semidiagnostic technique in which interior temperature and salinity distributions are forced toward observations [*Aumont et al.*, 1998; *Madec and Imbard*, 1996]. All models use similar geochemistry except for the biological pump. Both the MPI and IPSL models used the prognostic Hamburg Ocean Carbon Cycle Model, Version 3 (HAMOCC-3) parameterization of phosphate utilization described by *Maier-Reimer* [1993]. Princeton makes use of phosphate and alkalinity observations to determine the production and some aspects of the remineralization [*Murnane et al.*, 1999; *Sarmiento et al.*, 1995]. OCMIP-1 was designed to compare existing models with a minimum of modification. An ongoing OCMIP-2 exercise has as one of its elements a simulation using the same biology in all models to understand better the causes of differences between models such as those discussed in this paper. Further details of the models are given as each set of simulations is introduced.

3. Processes Determining the Sea-Air Flux of CO_2 and Interhemispheric Transport

In the following subsections, we discuss first a "potential solubility" model that enables us to directly compare the combined impact of heat and water fluxes on the sea-air CO_2 flux in

Table 1. Details of the Ocean Carbon Cycle Models Participating in the Ocean Carbon Model Intercomparison Project

	Princeton	IPSL	MPI
Model[a]			
Type	PE (MOM)	PE (OPA7)	LSG
Tracer run	on-line	off-line	off-line
Grid			
Horizontal	96 x 40	180 x 150	72 x 72
Vertical	12	30	22
Type[b]	B	C	E
Physics			
Forcing	prognostic	"semidiagnostic"	prognostic
Numerics (accuracy)	1st, 2nd	2nd	-
Free surface	no	no	yes
Advection scheme	centered difference	flux corrected transport	upstream
Seasonality	no	yes	yes
Mixing[c]			
Vertical	explicit	Turbulent Kinetic Energy Model (1.5 order)	numerical + explicit
Horizontal	1000-5000 $m^2 s^{-1}$	2000 $m^2 s^{-1}$	200 $m^2 s^{-1}$ + numerical
Chemistry[d]			
Virtual fluxes	yes	yes	no
Biological scheme	see text	HAMOCC-3	HAMOCC-3

Full descriptions of the models are given by *Maier-Reimer* [1993] for MPI (Max-Planck Institut), *Sarmiento et al.* [1995] and *Murnane et al.* [1999] for Princeton, and *Madec and Imbard* [1996] and *Aumont et al.* [1998] for IPSL (Institut Pierre Simon Laplace). The Princeton OCCM uses the GFDL ocean circulation model as developed by *Toggweiler et al.* [1989a].

[a]PE indicates primitive equation, MOM is Modular Ocean Model [*Pacanowski et al.*, 1993], OPA7 is Océan Parallelisé version 7, and LSG is Large-Scale Geostrophic model. On-line and off-line refer to whether the tracer simulations were done simultaneously with the prediction of the ocean circulation (on-line) or using average transport fields obtained from a prior circulation simulation.

[b]Grid types are as defined by *Arakawa* [1972].

[c]Numerical refers to numerical diffusion caused by the upstream advection scheme.

[d]Carbon chemistry is as given by *Dickson and Goyet* [1994] with the CO_2 solubilities of *Weiss* [1974]. The virtual flux results from the rigid lid approximation in the Princeton and IPSL models, which does not permit water fluxes. Water fluxes are represented instead by a flux of salt and other tracers [*Murnane et al.*, 1999]. MPI has a free surface that permits water fluxes.

the different models. Biological processes are suppressed. The surface ocean CO_2 is forced to be in equilibrium with the atmosphere at all locations. The potential solubility model instantaneously loses CO_2 to the atmosphere in regions where the combined effect of the heat and water fluxes increases the CO_2 concentration. It instantaneously gains CO_2 in regions where these processes combine to dilute the surface concentration.

In the second "solubility" model, we add a finite "realistic" gas exchange to the potential solubility model. The finite sea-air gas equilibration time permits water to travel over long horizontal distances after the CO_2 concentration is increased or diluted by the effect of heat and water fluxes and before it re-equilibrates with the atmosphere. This causes a widening and reduction in magnitude of the sharp peaks and troughs of the potential solubility pump model.

The third topic we discuss is the effect of biological processes estimated by subtracting the solubility model from the "combined" model, which includes both the solubility model processes and the biological pump. An alternative way to isolate the biological effects would be to do a biological simulation with constant temperature and salinity at the surface ocean (i.e., no heat or water flux). Unfortunately, because of the nonlinearity of carbon chemistry, there is not a single choice of temperature and salinity that would give an unambiguous measure of the contribution of the biological pump in isolation. For the same reason, our method does not give a clean separation of the two pumps either. The addition of biology changes the surface chemistry in such a way as to modify the response to a given addition or removal of heat or water. It would be of interest to compare the two approaches in a future study.

The biological pump contribution has a zero net sea-air carbon flux, as it must in a steady state, but there are substantial regional fluxes comparable, in many areas, to the magnitude of the solubility model fluxes. Thus, the biological pump substantially alters the spatial distribution of sea-air CO_2 fluxes determined by heat and water exchange and by the finite gas exchange.

Finally, we discuss two additional processes that affect the interhemispheric asymmetry of atmosphere-ocean carbon fluxes: the river flux of carbon, and the impact of anthropogenic CO_2 uptake on the spatial distribution of sea-air CO_2 fluxes.

3.1. Potential Solubility Model

The potential sea-air flux of CO_2 is defined as the flux that would result if the CO_2 content of the surface ocean water equilibrated instantaneously with the atmosphere [cf. *Keeling et al.*, 1993; *Watson et al.*, 1995]. The equation for the effect of a flux of heat is:

$$F_{CO_2}^{heat} = \frac{Q}{C_p}\frac{d[DIC]}{dT} = \frac{Q}{C_p}\left(\frac{1}{R}\frac{[DIC]}{pCO_2}\frac{dpCO_2}{dT}\right), \quad (1)$$

where Q is the flux of heat from the atmosphere to the ocean, T is temperature, C_p is the heat capacity of water, and R is the Revelle or buffer factor. The conversion between heat and car-

bon fluxes is ~1 PW to 0.8 Pg C y^{-1} for an R of 10 and $d\ln(pCO_2)/dT = 0.0423$ deg^{-1} [*Takahashi et al.*, 1993].

The equation for the effect of a flux of water from the atmosphere to the ocean (e.g., by evaporation, rainfall, and river runoff) is

$$F_{CO_2}^{water} = F_{H_2O}[DIC]\gamma$$

$$\gamma = \frac{\partial \ln[DIC]}{\partial \ln pCO_2}\left(\frac{\partial \ln pCO_2}{\partial \ln S} + \frac{\partial \ln pCO_2}{\partial \ln[Alk]} + \frac{\partial \ln pCO_2}{\partial \ln[DIC]}\right) \quad (2)$$

$$\cong \frac{1}{10}(1 - 9.4 + 10) = 0.16,$$

where F_{H_2O} is the flux of water in m^3 s^{-1}, S is salinity, and Alk is alkalinity. The derivatives are evaluated using results from the Geochemical Ocean Sections (GEOSECS) global mean temperature, salinity, DIC and Alk obtained from *Takahashi et al.*, [1981]. The $\partial \ln pCO_2/\partial \ln[Alk]$ derivative includes the effect of changes in the borate concentrations. A water input of 1 Sv (10^6 m^3 s^{-1}) reduces the ocean pCO_2 and therefore gives rise to a potential CO_2 gain from the atmosphere of 0.13 Pg C y^{-1}. A direct calculation of γ gives 0.17 for global mean properties, 0.18 for average warm water in the region between 45°S and 45°N, and 0.12 for mean cold water poleward of these latitudes.

The MPI and Princeton models are able to diagnose the potential CO_2 fluxes directly from (1) and (2) using the heat and water fluxes in the surface layer of the model. The MPI results discussed below come from such a calculation. However, the IPSL model has interior sources and sinks of heat and salt that arise from the semidiagnostic technique used to force model-predicted temperature and salinity toward the observations in the interior of the ocean. When water parcels affected by these interior processes outcrop at the surface, their carbon content will be out of equilibrium with the atmosphere even if there is no in situ sea-air flux of heat or water. In other words, the interior sources and sinks of heat and water masquerade as surface sources and sinks in their effect on the sea-air CO_2 flux. The only way to estimate the potential CO_2 fluxes in the IPSL model is therefore to do an actual "potential solubility" model simulation with equilibration of surface CO_2 with the atmosphere each time step. Note that the sea-air equilibration in an OCCM simulation cannot be instantaneous owing to the finite time step. Thus, the surface layer of 10 m thickness in the IPSL model has a ventilation timescale equal to the time step of 12 hours. In the Princeton model the potential flux was calculated by using (1) and (2), as well as by model simulation with such sea-air equilibration each time step (ventilation time of 1.5 days for the 50 m surface layer). Results from both approaches were virtually identical. The Princeton results given in this section are from the model simulation.

The potential solubility model used by IPSL and Princeton solves the full set of carbon system equations. Solving these equations requires specifying the temperature, salinity, and the concentration of two carbon system variables. The temperature and salinity are as predicted by the model. The two carbon system variables used are alkalinity and total carbon. IPSL fixes alkalinity at the observed salinity normalized global mean of 2374 μmol kg^{-1} [*Takahashi et al.*, 1981]. Princeton uses the same global mean value but allows the local alkalinity to vary in proportion with the salinity. Because biological processes that remove $CaCO_3$ from the surface are not included in the potential solubility model, the surface alkalinity is higher than observed.

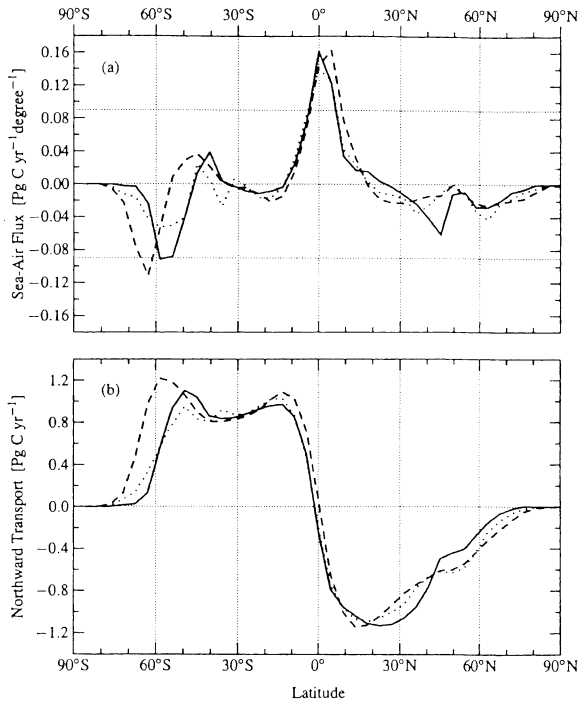

Figure 1. (a) Annual mean sea-air CO_2 fluxes from the potential solubility model. (b) Annual mean northward CO_2 transport in the potential solubility simulation. The solid line is the IPSL model, the dashed is the MPI model, and the dotted is the Princeton model.

The total carbon distribution in the IPSL and Princeton models is predicted by forcing the surface pCO_2 to be in equilibrium with the preindustrial atmospheric pCO_2 of 278 ppm at each time step. A final steady state total carbon distribution is obtained by running the model forward in time, permitting the surface total carbon concentrations to propagate into the interior and gradually modify the initial interior concentrations. A steady state solution is achieved when the global integral of the sea-air flux of CO_2 is zero; that is, the interior concentrations are unchanging. In practice, the models are run only until the global flux is below a small threshold value. To achieve this goal, the higher resolution model of IPSL used a new acceleration technique [*Aumont et al.*, 1998].

Equations (1) and (2) show that the potential sea-air CO_2 flux directly reflects the effect of heat and water fluxes across the sea-air interface. The separate analysis of the impact of Q and F_{H_2O} by *Murnane et al.* [1999] shows that the heat flux is by far the dominant process in determining the total F_{CO_2} in the potential solubility model. The discussion in this section thus refers predominantly to features in the heat flux distribution.

The prominent features of the zonal integral of the sea-air flux of CO_2 are the loss of CO_2 to the atmosphere in the tropics and the gain of CO_2 in high latitudes of both hemispheres (Figure 1a). The loss in the tropics is associated with heating in this region, and the gain in the high latitudes is due to cooling. The models follow each other closely except in the

Table 2. Northward Transport of Carbon at the Equator

	Princeton	IPSL	MPI
	Potential Solubility Model		
Atlantic	-0.50	-0.40	-0.50
Indo-Pacific	0.33	0.17	0.58
Global	-0.17	-0.23	0.08
	Solubility Model		
Atlantic	-0.24	-0.24	-0.22
Indo-Pacific	0.31	0.24	0.33
Global	0.07	0.00	0.11
	Combined Model		
Atlantic	-0.17	-0.18	-0.12
Indo-Pacific	0.05	0.08	0.15
Global	-0.12	-0.10	0.04
	Combined Model + Bering Strait Contribution[a]		
Atlantic	-0.80	-0.81	-0.75
Indo-Pacific	0.68	0.71	0.78
Global	-0.12	-0.10	0.04

The transport of carbon is given in Pg C y^{-1}.

[a]The carbon transport around the North and South American continents that is due to the flow through the Bering Strait is estimated to be 0.63 Pg C y^{-1} (P.M. Haugan and L. Lundberg, personal communication, 1996). Both the IPSL and MPI models simulate this transport directly. The solubility model and combined model results reported above for IPSL and MPI have had this contribution removed.

Southern Ocean, where the MPI model shows a poleward shift of the region of maximum CO_2 uptake and the Princeton model shows a smaller uptake than the other two. The peak uptake rate of the MPI model in the Southern Ocean is about twice that of the Princeton model. However, it decreases rapidly to the north and changes sign at about 55°S, almost 10° farther south than the other two models.

All the potential solubility models predict a small carbon transport across the equator, which is consistent with the nearly symmetrical sea-air fluxes on both sides of the equator (Figure 1b and Table 2). The southward transport at 15°N is more than 1 Pg C y^{-1} (Table 3), but most of this is lost to the atmosphere north of the equator. The only way to obtain a large southward transport of carbon in the potential solubility model would be if there were a substantial net northward transport of heat or southward transport of water. The 1 Pg C y^{-1} net southward transport hypothesized by *Keeling et al.* [1989] would require a cross-equatorial northward heat transport of ~1.2 PW.

A variety of observational and modeling studies supports the notion of a northward cross-equatorial transport of heat in the Atlantic Ocean [e.g., *Martel and Wunsch*, 1993; *Sarmiento et al.*, 1995]. The heat transport from our OCCMs implies a potential southward transport of carbon of ~0.5 Pg C y^{-1} in the Atlantic (Table 2). However, this is roughly counterbalanced by a northward transport in the Indo-Pacific, so that the final net cross-equatorial transport is small, about -0.17 Pg C y^{-1} for Princeton, -0.23 Pg C y^{-1} for IPSL, and +0.08 Pg C y^{-1} for

Table 3. Global Northward Transport of Carbon

	Princeton	IPSL	MPI
	15°N		
Potential solubility model	-1.07	-1.03	-1.14
Gas exchange contribution	0.45	0.41	0.67
Biological pump	0.01	-0.05	0.04
Total (combined model)	-0.61	-0.66	-0.43
	Equator		
Potential solubility model	-0.17	-0.23	0.08
Gas exchange contribution	0.24	0.23	0.03
Biological pump	-0.19	-0.10	-0.07
Total (combined model)	-0.12	-0.10	0.04
	15°S		
Potential solubility model	1.02	0.97	1.09
Gas exchange contribution	-0.23	-0.20	-0.33
Biological pump	-0.20	-0.07	-0.26
Total (Combined model)	0.59	0.70	0.50
	30°S		
Potential solubility model	0.88	0.85	0.83
Gas exchange contribution	0.11	0.14	0.04
Biological pump	-0.56	-0.22	-0.53
Total (combined model)	0.43	0.77	0.34

The transport is given in Pg C y^{-1}. The "gas exchange contribution" is found by subtracting the solubility model from the potential solubility model and thus includes the effect of gas exchange on the solubility pump only. The biological pump is the difference between the combined and solubility models.

MPI (Table 2). We know of no ocean models with realistic topography and boundary conditions that predict a global cross-equatorial heat flux of more than a few tenths of a petawatt, including the high-resolution world ocean model of *Semtner and Chervin* [1992]. Data-based estimates are also mostly small, giving global cross equatorial heat transports of only a few tenths of a petawatt [*Talley*, 1984; *Hastenrath*, 1982; *Trenberth and Solomon*, 1994; cf. *Murnane et al.*, 1999]. The largest data-based heat fluxes are those obtained by *da Silva et al.* [1994], who estimate a northward flux of ~0.7 PW in the Atlantic and ~0.7 PW in the Pacific. Combined with a southward flux of ~0.7 PW in the Indian Ocean, this study gives a northward global flux of 0.7 PW. The *da Silva et al.* [1994] result is much closer to the value of 1.2 PW required in order to get a 1 Pg C y^{-1} southward flux of carbon. However, as we shall see in the following section, the actual solubility pump carbon transport is much smaller than the potential solubility pump transport.

The large uptake of CO_2 in the Southern Ocean of the MPI model (Figure 1a) requires a correspondingly large northward transport of carbon in the ocean (Figure 1b). Note that the CO_2 loss due to heat uptake between 40° and 60°S compensates for the CO_2 gain due to the heat loss south of that region. By about 40°S, the northward transport of the MPI model is virtually identical to that from the Princeton and IPSL models (compare transport at 30°S shown in Table 3).

To summarize, except for the highest latitudes of the Southern Ocean, the three models included in the potential solubility model comparison have similar zonal integral sea-air CO_2 fluxes and meridional CO_2 transports. This occurs despite large differences in the model physics. All three models predict a small carbon transport across the equator. The only way this could be increased is if the models predicted a substantially larger northward transport of heat in the global ocean. This is not supported by the observations, most of which agree with the ocean model results. Even the larger *da Silva et al.* [1994] heat transport is not large enough to give 1 Pg C y^{-1}.

3.2. Solubility Model

The solubility model is identical to the potential solubility model except for the addition of a "realistic" gas exchange formulation. The atmospheric pCO_2 is fixed at its observed preindustrial value of 278 ppm, and CO_2 is allowed to invade or evade the ocean until the globally integrated flux is 0. The IPSL, MPI, and Princeton models all use a modified form of the wind speed gas exchange coefficient model of *Wanninkhof* [1992, equation 5] (with the constant d set to 0.315) with wind speeds given by J. Boutin and J. Etcheto (personal communication, 1995). See *Orr et al.* [2000] for a full explanation.

The equilibration of surface ocean CO_2 with the atmosphere takes of the order of 1 year for a 75 m mixed layer [cf., *Broecker and Peng*, 1974]. This long delay can lead to a substantial mismatch between the solubility model fluxes and the potential solubility model fluxes. For example, the poleward Ekman transport near the equator rapidly displaces water poleward in both hemispheres before equilibration with the atmosphere can occur. This lateral spreading reduces the peak loss rate at the equator by more than 50% (compare Figures 2a and 1a; note the change in vertical scale).

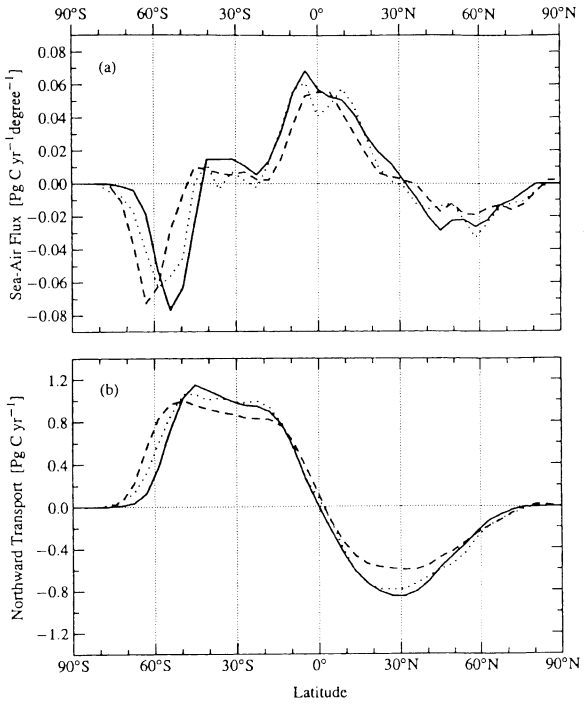

Figure 2. (a) Annual mean solubility model sea-air CO_2 fluxes. (b) Annual mean northward CO_2 transports in the solubility model. The solid line is the IPSL model, the dashed is the MPI model, and the dotted is the Princeton model.

The gas exchange contribution reduces the southward transport at 15°N by almost 50% (Table 3). Interestingly, the gas exchange contribution at 15°S is about half that at 15°N (Table 3). This is presumably a result of slower thermocline ventilation (i.e., longer residence times of water in the surface mixed layer) in the southern than in the northern subtropics. The longer residence time of water in the southern surface mixed layer permits sea-air equilibration of CO_2 to occur, thus bringing the solubility model closer to the potential solubility model results. Note also that the MPI model has a larger gas exchange contribution at 15°S and 15°N than the other models (Table 3). This may be caused by the upstream advection scheme used in this model, which can lead to large apparent mixing, i.e., more rapid thermocline ventilation.

The Princeton model has a dip in the CO_2 loss at the equator that is absent from the other models (Figure 2a). The Princeton model differs from the others in that it lacks seasonal forcing. The equatorial minimum in CO_2 reflects the fact that the annual mean wind speeds are substantially lower at the equator than to the north and south. The seasonal migration of the Inter-Tropical Convergence Zone in the seasonally forced models may be a factor in reducing the influence of this feature.

Another notable feature in the sea-air flux distributions is that the large uptake peak in the Southern Ocean of the MPI model has decreased and now looks more like the others (Figure 2a). Also of interest is the band between ~30° and 45°S where the models all show a small loss of CO_2 to the atmosphere in a region where cooling might be expected to lead to CO_2 uptake. In the Princeton model, unusually large upwelling that occurs along western boundaries causes this loss of

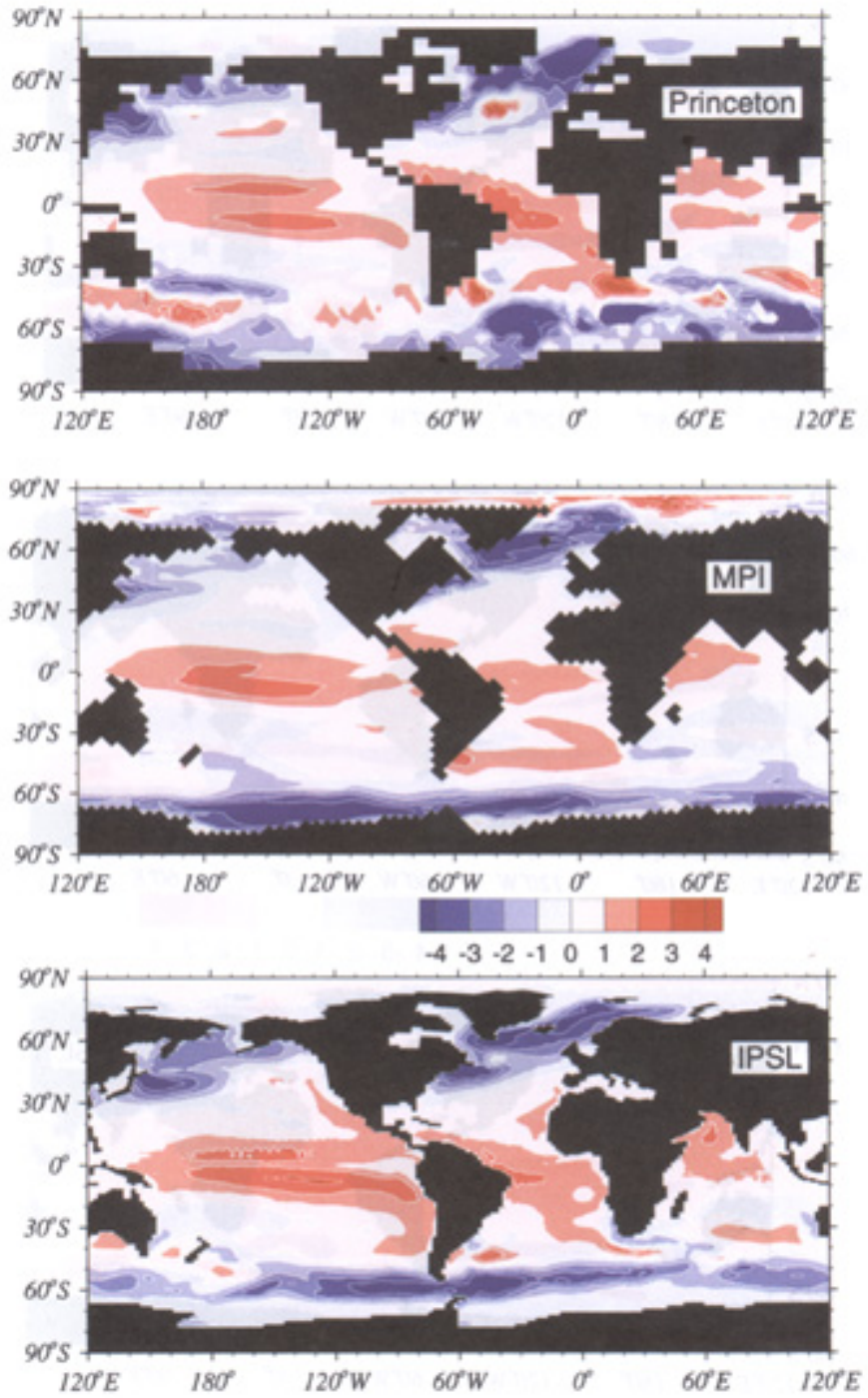

Plate 1. Maps of annual mean sea-air CO_2 fluxes in the solubility model.

CO_2 to the atmosphere. The upwelling is a consequence of unrealistically strong horizontal mixing across the steeply sloping isopycnals of the western boundary currents [*Veronis*, 1975; *Toggweiler et al.*, 1989b]. The IPSL and MPI models have similar features.

Maps of the sea-air CO_2 fluxes show that the regions of high CO_2 uptake in the Southern Ocean region of the MPI model are concentrated in two broad bands near the Ross and Weddell Seas (Plate 1). The dominant features of the Southern Ocean region of the Princeton model are several regions of exceptionally high CO_2 uptake. These features are characteristic of all the simulations carried out with the GFDL ocean circulation model using annual mean wind and annual mean surface temperature and salinity forcing. They result from high heat

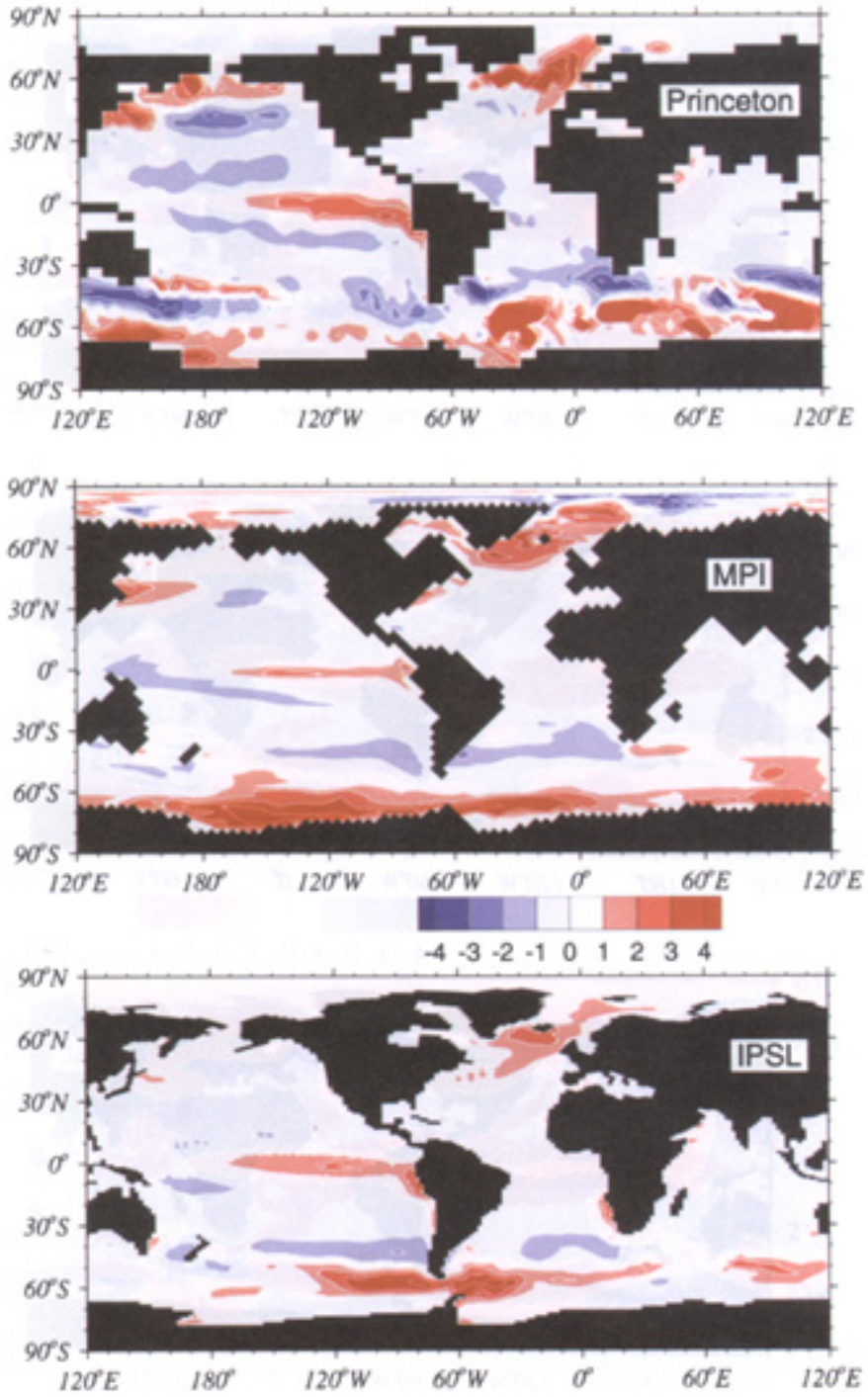

Plate 2. Maps of annual mean sea-air CO_2 fluxes due to the biological pump.

loss over convective plumes whose location is fixed. The convective plumes are greatly reduced in versions of the GFDL model that include isopycnal mixing. Note that the convection plumes in the Princeton/GFDL model occur at lower latitudes than the processes that give rise to the peak uptake features in the MPI model. The dominant uptake in the Southern Ocean of the IPSL model is northward of that in the MPI model and more homogeneous than the convective plume distribution in the Princeton model.

An interesting feature of the IPSL model is the loss of CO_2 to the atmosphere in near shore upwelling regions (Plate 1). These occur primarily off the west coast of North and South America and Africa, as well as a few other regions off Argentina and the Arabian peninsula. These features are most

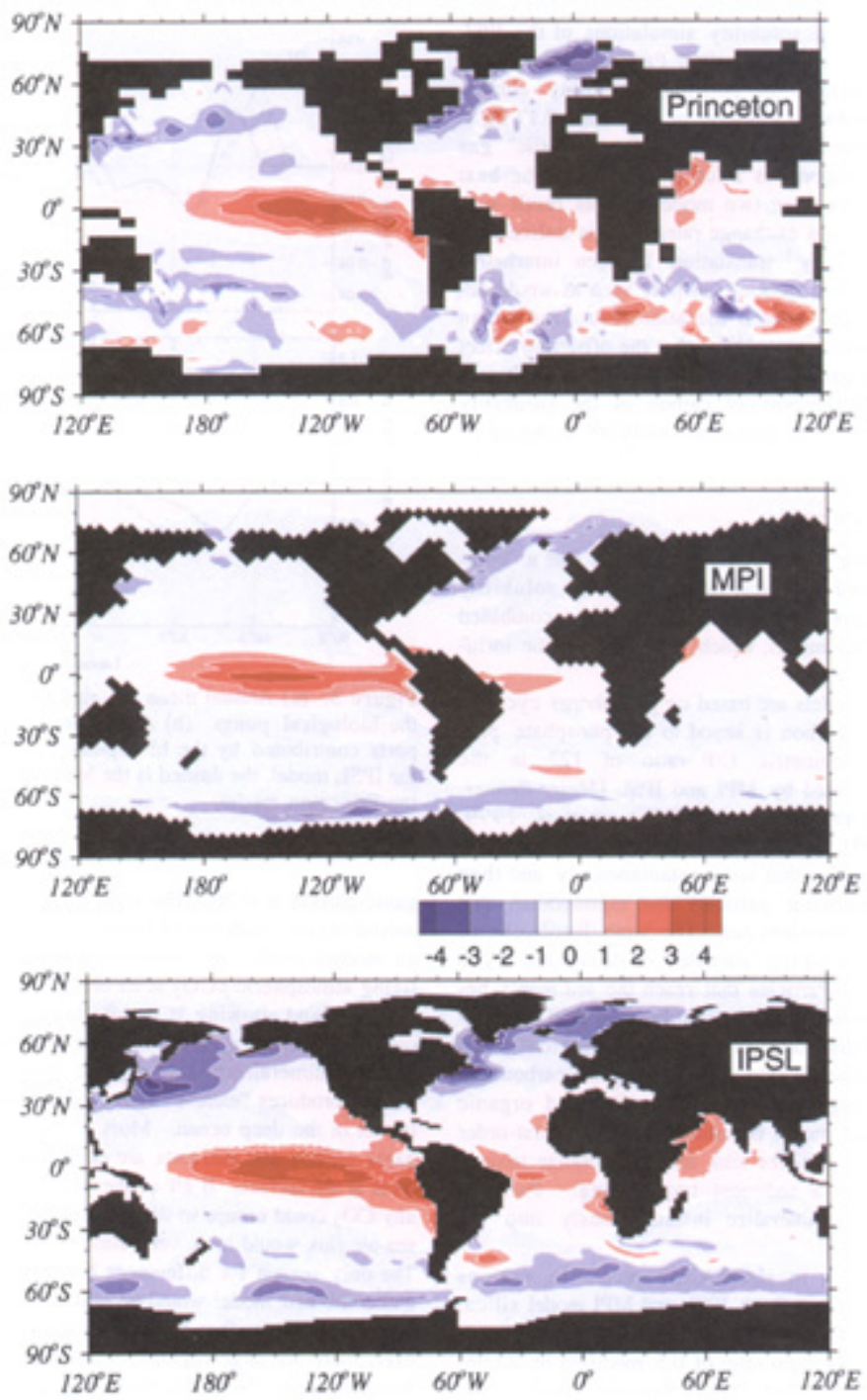

Plate 3. Maps of annual mean sea-air CO_2 fluxes in the combined model.

likely a consequence of the higher horizontal resolution in the IPSL model. The Princeton model has small uptake maxima at about 35°S and 35°N (most prominent in the potential solubility model, Figure 1a). These are due primarily to features off the east coast of Asia, North America, and South America (Plate 1), where water from lower latitudes is cooled. The IPSL model shows similar features, particularly in the Northern Hemisphere. Given the large differences in the regional distribution of sea-air fluxes (Plate 1), it is remarkable how little difference one sees in the zonal means (Figure 2a).

The similarity of the solubility simulation sea-air CO_2 fluxes of the different models translates into virtually identical curves of northward carbon transport (Figure 2b). At the equator, the effect of gas exchange is greater in the IPSL and

Princeton models than in the MPI model (Table 3). The cross-equatorial transport in the solubility simulations of the IPSL and Princeton models is +0.00 and +0.07 Pg C y^{-1} (northward), respectively. By contrast, the potential solubility simulations gave a small southward transport of -0.23 and -0.17 Pg C y^{-1}, respectively (Table 2). The addition of a "realistic" gas exchange coefficient suppresses a full expression of the heat transport effect found in these two models. This result suggests that with realistic gas exchange rates there is unlikely to be a 1 PW to 0.8 Pg C y^{-1} translation between interhemispheric heat transport and carbon transport such as would occur if the gas exchange between the atmosphere and ocean mixed layer were instantaneous. Note that the offsetting effect of gas exchange is particularly large in the Atlantic Ocean, where the southward transport of carbon in the solubility pump is about half that of the potential solubility pump in all three models (Table 2).

3.3. Biological Pump

The next step in the model comparison study was a "combined" model that added biological processes to the solubility model. Here we discuss the difference between the combined model and the solubility model, which we ascribe to the influence of the biological pump.

All the biological models are based on phosphorus cycling. Production of organic carbon is keyed to the phosphate production with a stoichiometric C:P ratio of 122 in the HAMOCC-3 approach used by MPI and IPSL [*Maier-Reimer*, 1993] and 120 in the Princeton model [*Murnane et al.*, 1999, *Sarmiento et al.*, 1995]. HAMOCC-3 puts newly produced organic carbon into particles that sink instantaneously and then are converted to nonsinking particles that remineralize at a specified temperature dependent rate. The depth distribution of the conversion to nonsinking particles is determined by a sediment trap scaling. Particles that reach the sediments become nonsinking particles in the bottom layer in IPSL and enter a simple model of diagenesis in MPI. The Princeton model puts half the new production into dissolved organic carbon and half into particulate organic carbon. The dissolved organic matter of the Princeton model is remineralized as a first-order decay process, and the particles sink and remineralize instantaneously according to a sediment trap scaling. Particles reaching the bottom remineralize instantaneously into the bottom box of the model.

Production of $CaCO_3$ in HAMOCC-3 occurs in regions where silicate is not present (both IPSL and MPI model silica; Princeton does not). The $CaCO_3$ production is keyed to organic carbon, with a maximum ratio of 0.5 modified by a temperature dependent coefficient [*Maier-Reimer*, 1993]. The global mean $CaCO_3$ to organic carbon production is 0.22 in MPI and 0.25 in IPSL. Remineralization of $CaCO_3$ occurs exponentially with a 2 km depth scale, with sediment dissolution occurring in undersaturated regions. The Princeton model estimates $CaCO_3$ production and remineralization at each time step by forcing the horizontal average of the model predicted alkalinity toward its observed value at each depth level [*Murnane et al.*, 1999, *Sarmiento et al.*, 1995]. The local model prediction is then made using the global horizontal mean of the ratio of $CaCO_3$ to organic carbon production and consumption. The export ratio of $CaCO_3$ to particulate organic carbon is 0.26. The export ratio drops to 0.16 if dissolved organic matter is included. As in previous simulations, all models predict the atmosphere-ocean balance of CO_2 by fixing atmospheric pCO_2 at its observed preindustrial value of 278 ppm and allowing it to invade the ocean until the deep ocean DIC achieves an equilibrium concentration.

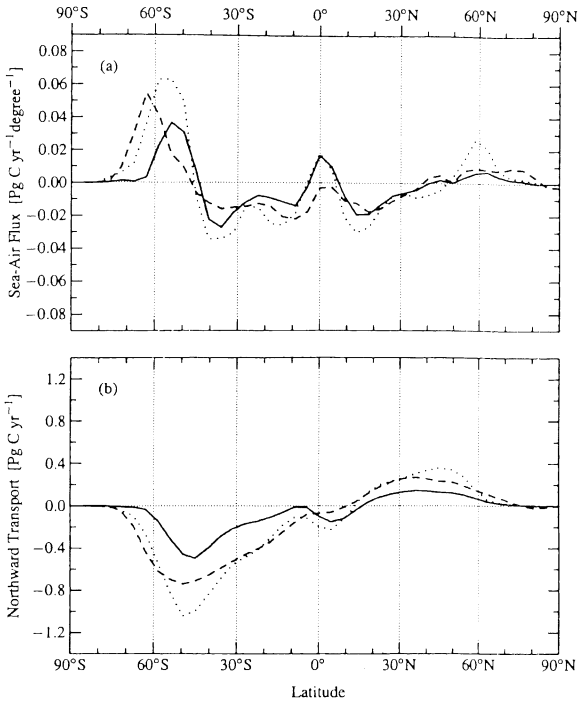

Figure 3. (a) Annual mean sea-air CO_2 fluxes contributed by the biological pump. (b) Annual mean northward CO_2 transports contributed by the biological pump. The solid line is the IPSL model, the dashed is the MPI model, and the dotted is the Princeton model.

The remineralization of organic matter and dissolution of $CaCO_3$ produces "excess" dissolved inorganic carbon and nutrients in the deep ocean. Most of the excess dissolved inorganic carbon and nutrients are consumed when deep water arrives at the surface. If all of the excess were consumed before any CO_2 could escape to the atmosphere, the surface ocean and sea-air flux would look very similar to the solubility model. The only reason for differences between the solubility model and combined model would be that the alkalinity distribution is lower at the surface in the biological pump model. However, there are large regions of the ocean, particularly in the North Atlantic, North Pacific, tropical Pacific, and Southern Ocean, where biological uptake is inefficient relative to the upward supply of excess carbon and nutrients. These regions lose excess CO_2 to the atmosphere (Figures 3a and Plate 2). In a steady state, this loss must be balanced by uptake in the remaining regions, namely the subtropics. We thus arrive at the biological pump pattern of Figure 3a and Plate 2. There is a large loss of CO_2 to the atmosphere in the high latitudes of the Southern Ocean and a more modest loss in the high latitudes of the Northern Hemisphere. The IPSL and Princeton models also have a loss in the tropics. The losses are balanced by uptake in the subtropics.

The overall structure of the biological pump sea-air CO_2 fluxes is similar in all three models, but the range between them is greater than in the potential solubility and solubility models. One of the major reasons for the difference between the IPSL and Princeton models is that the IPSL model has less convective overturning. This has the consequence that the biological pump in IPSL is able to take up a larger fraction of the nutrients and excess carbon brought to the surface by transport, most notably in the high latitudes of the Southern Ocean. There the IPSL biological pump model has a much lower loss to the atmosphere than the other models (Figure 3a). This is reflected in the southward transport across 30°S, which is half that of the other two biological pump models (Table 3). Note the different structures in the Southern Ocean sea-air CO_2 fluxes of the models, with a higher latitude peak in the MPI model than the others (Figure 3a). This reflects the different high latitude convective overturning patterns discussed previously (Plate 2), as well as differences in the way that $CaCO_3$ is parameterized. The $CaCO_3$ to organic carbon ratio of the MPI and IPSL models is low in the cold waters of the Southern Ocean. The Princeton model has the same ratio there as elsewhere, which leads to higher CO_2 outgassing.

The loss of excess biological pump CO_2 to the atmosphere in the Southern Ocean (Figures 3a and Plate 2) is supplied by a large southward transport of carbon (Figure 3b and Table 3). There is also a northward transport in the Northern Hemisphere as required to supply the loss in that region. Despite the need for a large oceanic transport of carbon to the Southern Ocean, the cross-equatorial transport is very small: -0.07 to -0.19 Pg C y^{-1} (Table 3). The CO_2 lost to the atmosphere in the Southern Ocean comes almost entirely from lower latitudes of the Southern Hemisphere. Note also the small convergence of carbon transport to supply the flux to the atmosphere at the Equator in the Princeton and IPSL models (Figure 3b).

3.4. Combined Model

The outstanding feature of the combined model sea-air flux is the substantial cancellation of the solubility model fluxes by the biological pump fluxes. The magnitude of the biological pump sea-air flux is comparable to that of the solubility model, particularly in the Southern Ocean (compare Figures 2a and 3a). The biological pump flux is also of opposite sign to that of the solubility model almost everywhere except the tropics. Consequently, the combined model flux is relatively small everywhere except the tropics (Figure 4a and Plate 3). The cancellation of the biological pump by the solubility pump is particularly dramatic in the Southern Ocean, especially in the Princeton model. The wide range between the sea-air fluxes of the three biological pump simulations carries over into the combined model. The Princeton model has a large uptake at ~35°S owing to unrealistic upwelling features along the eastern boundaries of the continents discussed in Section 3.2. The other two models have a peak uptake at ~55°S because the biological pump is not large enough to cancel the entire solubility pump.

The sea-air flux features of the combined model are all reflected in the carbon transport (Figure 4b). Adding all the contributions together, one sees that the total carbon transport across the equator remains small, ranging from -0.12 to +0.04 Pg C y^{-1} (Table 2). All terms are small in the MPI model, but

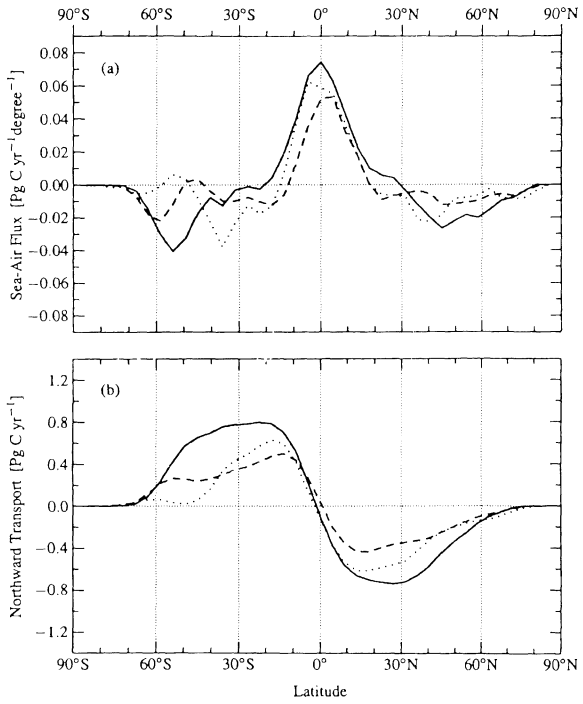

Figure 4. (a) Annual mean sea-air combined model CO_2 fluxes. (b) Annual mean northward CO_2 transports in the combined model. The solid line is the IPSL model, the dashed is the MPI model, and the dotted is the Princeton model.

the Princeton and IPSL models have a relatively large southward potential solubility plus biological pump transport (-0.36 and -0.33 Pg C y^{-1}, respectively) that is mostly offset by the solubility pump gas exchange contribution (0.24 and 0.23 Pg C y^{-1}, respectively). The transport at 15°N is southward in all models but smaller in the MPI model owing primarily to the larger gas exchange contribution (more rapid thermocline ventilation; Table 3). The transport at 15° and 30°S is to the north in all these models but greater in the IPSL model owing to the smaller biological pump contribution discussed in the previous section.

Table 2 also shows how the basin transports are affected by the net water transport of 0.8 x 10^6 m^3 s^{-1} northward through the Bering Strait [*Coachman and Aagard*, 1988; *Roach et al.*, 1995]. This net water transport gives a northward carbon transport of 0.63 Pg C y^{-1} [*Holfort et al.*, 1998] that must be added to the carbon transport around both American continents. This is based on a dissolved inorganic carbon concentration of 2020 to 2040 μmol kg^{-1}, and negligible dissolved organic carbon [*Anderson et al.*, 1990]. The combined model transport plus Bering Strait contribution give a very large southward transport of ~0.8 Pg C y^{-1} in the Atlantic Ocean. However, this is counterbalanced by a northward transport in the Indo-Pacific and thus has no net impact on the global interhemispheric transport. The Atlantic Ocean carbon transport estimates of *Keeling et al.* [1989], *Broecker and Peng* [1992], and *Keeling and Peng* [1995] do not include the net carbon transport component due to the Bering Strait throughflow. They should thus be compared with the combined model results only.

Table 4. Global Northward Transport of Carbon Across the Equator

	Princeton	IPSL	MPI
Potential solubility model	-0.17	-0.23	0.08
Gas exchange contribution	0.24	0.23	0.03
Biological pump	-0.19	-0.10	-0.07
River input contribution	-0.25	-0.25	-0.25
Total (combined model + rivers)	-0.37	-0.35	-0.21

The transport is given in Pg C y^{-1}.

4. Discussion

All three OCCM combined models presented here fail to simulate a significant cross-equatorial transport of carbon during preindustrial times (Table 2). However, an additional contribution to the ocean carbon budget that needs to be taken into consideration is the input of carbon by rivers [*Sarmiento and Sundquist*, 1992]. The river flux of carbon is due primarily to terrestrial uptake via photosynthesis and chemical weathering in the Northern Hemisphere. Once in the ocean, it may be transported southward before being returned to the atmosphere.

An explicit simulation of the river flux was not included in the OCMIP simulations because good river flux estimates were not available when the study was initiated. However, subsequent research [*Amiotte-Suchet and Ludwig*, 1998; *Ludwig et al.*, 1996; *Bluth and Kump*, 1994; *Gibbs and Kump*, 1994] provides for each river basin the carbon discharge for both inorganic carbon (DIC) and organic carbon (DOC and POC). *Aumont* [1998] has included this riverine input of carbon in his recent global ocean simulation of the global carbon cycle with the IPSL model. His current estimate for the riverine contribution to the cross-equatorial transport of carbon is -0.25 ± 0.08 Pg C y^{-1}, i.e., southward. The range depends on the assumed rate of remineralization of organic carbon brought in by the rivers. About two-thirds of this transport occurs in the Atlantic Ocean, and one-third occurs in the Indian and Pacific Oceans.

Table 4 shows that the riverine contribution increases the global southward carbon transport to between 0.2 and 0.4 Pg C y^{-1}. The southward flux of riverine carbon in the Indo-Pacific almost balances the northward combined model transport shown in Table 2. Essentially all of the southward transport occurs in the Atlantic Ocean. The three global ocean model transport estimates, when shifted by the *Aumont* [1998] riverine carbon transport, account for only one-third to one-half the Atlantic Ocean transport postulated by *Keeling et al.*, [1989]. However, they agree with the Atlantic Ocean estimate of 0.4 Pg C y^{-1} obtained by *Keeling and Peng* [1995] in their update of the *Broecker and Peng* [1992] study.

Our dissection of the carbon transport into components makes it possible for us to analyze what determines the cross-equatorial transport. We consider first the effect of heat transport. The potential solubility model results summarized in Table 2 show that the northward transport of heat in the model Atlantic Oceans is large enough to drive a southward carbon transport of 0.4-0.5 Pg C y^{-1}. However, this is counterbalanced by a northward carbon transport in the Indian and Pacific Oceans. Furthermore, the long period of time that it takes for CO_2 to equilibrate between the atmosphere and mixed layer of the ocean leads to a decoupling of the heat and CO_2 fluxes. The CO_2 flux is therefore lower than would be expected from the heat flux (compare solubility with potential solubility model results in Table 2). In the end, the solubility models simulate an interhemispheric carbon transport of between 0.00 and +0.11 Pg C y^{-1}.

The biological pump also contributes to the southward carbon transport. Its contribution depends on the correlation between meridional transport and that portion of the variation in water column DIC concentration that results from the biological pump. Both the meridional transport and the DIC distribution contribute uncertainty. However, despite large differences in both of these between the different models, the models agree that the overall contribution remains small.

An additional contribution to the interhemispheric carbon balances that we consider is the role of anthropogenic CO_2 uptake by the ocean. The uptake of anthropogenic carbon was simulated in the OCCMs by increasing the atmospheric CO_2 according to observations from 1765 to 1990 [*Orr et al.*, 2000]. The total uptake in 1990 ranges between 1.69 for the

Table 5. Sea-Air CO_2 Fluxes in 1990 Including Anthropogenic and Riverine Carbon

	Princeton	IPSL	MPI
	Equator to 90°N		
Preindustrial without rivers	-0.12	-0.10	0.04
Riverine outgassing	0.21	0.21	0.21
Anthropogenic	-0.88	-0.59	-0.78
Subtotal	-0.80	-0.48	-0.53
	90°S to Equator		
Preindustrial without rivers	0.12	0.10	-0.04
Riverine outgassing	0.43	0.43	0.43
Anthropogenic	-1.57	-1.10	-1.05
Subtotal	-1.01	-0.57	-0.66
	90°S to 90°N		
Riverine outgassing	0.64	0.64	0.64
Anthropogenic	-2.45	-1.69	-1.83
Total	-1.81	-1.05	-1.19

Fluxes are given in Pg C y^{-1}.

Table 6. Sea-Air Fluxes Estimated by Previous Studies

Study	Time Period	Northern Hemisphere	Southern Hemisphere	Global
		Analysis of Atmospheric Observations		
Keeling et al. [1989]	1984	-1.9	-0.4	-2.3
Ciais et al. [1995b]	1990-1992	-0.9	-1.3	-2.2
Keeling et al. [1996][a]	1991-1994	-1.0	-0.7	-1.7
		Analysis of Ocean Observations		
Takahashi et al. [1999][b]	1995	-0.7	-1.4	-2.2

Fluxes are given in Pg C y^{-1}. The analysis of atmospheric observations gives an estimate that is synoptic in time. The ocean observation estimate is based on data gathered over a long period of time.

[a]Based on the numbers that *Keeling et al.* [1996] found to be consistent with their atmospheric O_2 and CO_2 measurements. They include an uptake of 0.4 Pg C y^{-1} in the North Atlantic and release in the Southern Hemisphere, to which has been summed a global anthropogenic uptake of 1.7 Pg C y^{-1} scaled regionally using the *Sarmiento et. al.* [1992] model results.

[b]Results obtained with the wind speeds of *Wanninkhof* [1992]. This estimate is an update of an earlier study by *Takahashi et. al.* [1997] for the period of 1990. The earlier study gave a Northern Hemisphere uptake of 0.6 Pg C y^{-1} and a Southern Hemisphere uptake of 0.8 Pg C y^{-1}, for a global total of 1.4 Pg C y^{-1} (after adjustment to the gas exchange coefficient and wind field of the *Takahashi et al.,* [1999] study). The increase in oceanic uptake of the more recent results is due primarily to more data, particularly in the Southern Hemisphere, but also in part to the increase in atmospheric CO_2 between 1990 and 1995.

IPSL model and 2.45 Pg C y^{-1} for the Princeton model (Table 5). The uptake in the MPI model is 1.83 Pg C y^{-1}.

Orr et al. [2000] discuss the differences in total anthropogenic CO_2 uptake between the OCCM models, including comparisons with observations. A part of the difference is due to a greater penetration of anthropogenic carbon in the Southern Ocean of the Princeton model. Comparisons of model results with observations suggest that vertical penetration in this region is too high in the Princeton model. However, this is not the full explanation, as the MPI model also has deep tracer penetration in the Southern Ocean (though much farther to the south), but the total anthropogenic uptake is smaller. Analysis of the bomb radiocarbon uptake and comparison of this with observations also gives ambiguous results. The IPSL model gives a smaller radiocarbon penetration depth than the Princeton model, which is consistent with its smaller anthropogenic carbon uptake. However, the MPI model has the same radiocarbon penetration depth as the Princeton model despite having a smaller anthropogenic carbon uptake.

Another way of analyzing the anthropogenic carbon simulations is to compare the sea-air fluxes with independent estimates. We first consider the global integral sea-air flux, which consists of the global anthropogenic carbon uptake plus the riverine outgassing contribution of 0.64 Pg C y^{-1}. Summing these two gives a global sea-air flux of -1.81 Pg C y^{-1} for the Princeton model, -1.05 Pg C y^{-1} for the IPSL model, and -1.19 Pg C y^{-1} for the MPI model (Table 5). Previous independent estimates of the sea-air flux based on analyses of atmospheric and ocean observations range from -1.7 to -2.3 Pg C y^{-1} (Table 6). Only the Princeton model is within the range of these independent estimates. The other two ocean models, IPSL and MPI, have net oceanic uptakes that are smaller than independent estimates by between 0.5 and more than 1 Pg C y^{-1}.

The disagreement between estimates of global integral sea-air fluxes has many possible explanations. One is simply interannual variability, which the *Le Quéré et al.* [2000] model study shows may have a magnitude of ±0.4 Pg C y^{-1}. The independent analyses in Table 6 represent a range of timescales. For example, the *Ciais et al.* [1995b] number given there is an average over 3 years of analysis, which have total ocean uptakes of between -1.0 and -3.1 Pg C y^{-1}. However, other possible interpretations exist. One is that the estimated magnitude of the riverine outgassing contribution is too high. Another is that problems with the ocean circulation models are leading to unrealistic results. A more complete understanding of the models will require a more detailed analysis of the regional behavior of the tracers, as well as additional model simulations. The availability of the more complete World Ocean Circulation Experiment (WOCE) and Joint Global Ocean Flux Study (JGOFS) global survey data sets, particularly in the Southern Ocean region, will be of great help in this effort.

The hemispheric breakdown of previous estimates of the sea-air fluxes is given in Table 6. It is consistent with our earlier analysis of the interhemispheric transport in showing that the extremely large *Keeling et al.*, [1989] estimate of Northern Hemisphere uptake is outside the range of other work. If their estimate of -1.9 Pg C y^{-1} is excluded, the ocean model and data based results are in reasonable agreement, with a range of -0.5 to -1.0 Pg C y^{-1}. The IPSL and MPI models are at the lower end of this range. The agreement in the Southern Hemisphere is not as good, with a range of -0.6 to -1.4 Pg C y^{-1}. The *Keeling et al.,* [1989] estimate is slightly lower than this range at -0.4 Pg C y^{-1}. The IPSL and MPI models are again at the lower end of the range at -0.6 Pg C y^{-1}.

Overall, it appears that the ocean models do not contribute to the enhancement of the Northern Hemisphere relative to Southern Hemisphere carbon uptake suggested by analyses of atmospheric observations. This must be due primarily to terrestrial processes. All the independent estimates shown in Table 6, except that of *Keeling et al.,* [1989], also show little or no enhancement of the Northern Hemisphere sink over the Southern Hemisphere ocean carbon sink.

It is interesting that the models are in reasonably good agreement almost everywhere except in the Southern Ocean. This is particularly surprising in view of the substantially different physics of the three models (Table 1). The Princeton and IPSL models use a primitive equation approach, whereas the MPI model uses a large-scale geostrophic approach. The IPSL model is semidiagnostic; that is, it forces the model pre-

dicted temperature and salinity towards observations. The Princeton model is nonseasonal, whereas the others include seasonal forcing.

Yet there are important differences that deserve further study. First, the thermocline ventilation rate interacts with the slow gas exchange rate to give a significantly different behavior of the "gas exchange contribution" in the MPI model than in the other two (Table 3). The ventilation rate can be tested with tracers. Second, the biology also gives very different results in all three models (Figure 3a). This is clearly an area of frontier research to which projects like JGOFS can contribute. Third, the Southern Ocean is very different in all three models. The data constraints on deep-water formation processes and nutrient and carbon distributions are very limited in this region. New observations of tracers, hydrography, nutrients, the carbon system, and biogeochemical processes are beginning to become available from WOCE and JGOFS. These should help to improve the models in this area, which has been shown to be critical to the sea-air balance of carbon [e.g., *Sarmiento et al.,* 1998, *Sarmiento and Le Quére*, 1996, *Sarmiento et al.,* 1992].

Stephens et al. [1998] have recently introduced a new tracer that should prove very useful in improving our understanding of the ocean-atmosphere behavior of biogeochemical gases. Atmospheric potential oxygen, which is a combination of CO_2 and O_2, is conservative with respect to the land biosphere. It therefore traces sea-air fluxes and fossil fuel burning. In their analysis of a limited atmospheric data set, *Stephens et al.* [1998] suggest that the Princeton and MPI models (as well as a third model developed at Lawrence-Livermore) significantly underestimate the interhemispheric transport of carbon and oxygen. They have a number of hypotheses as to what may be wrong with the ocean models, including the possibility that they have too much convection in the Southern Ocean and/or too much upwelling at the Equator. The IPSL model is very different from the other two models in that it has very little convection in the Southern Ocean and much smaller upwelling in the tropics. However, its simulation of the carbon transport and of APO does not differ significantly from that of the other two models [*Aumont*, 1998]. The issues raised by the *Stephens et al.* [1998] study, including the fact that the atmospheric data set is somewhat limited, remain to be resolved.

Acknowledgments. The Ocean Carbon-cycle Model Intercomparison Project (OCMIP) is an activity of IGBP/GAIM. We thank B. Moore and D. Sahagian for running the GAIM office, and NSF and NASA for sponsoring the GAIM contributions to OCMIP. J. L. Sarmiento and R. Murnane were supported by a grant from the NOAA Office of Global Programs (NA56GP0439) and received computer support from GFDL/NOAA through the generosity of J. Mahlman. P. Monfray, O. Aumont, and J. Orr were funded by the European Community Environment and Climate Programme (ENV4-CT95-0132), with computing support from the French CEA/DSM and CNRS/IDRIS. E. Maier-Reimer was supported by a grant from the German BMBF (V-044-TIEFBIT). Reviews by Fortunat Joos, Britt Stephens, and an anonymous reviewer were very helpful.

References

Amiotte-Suchet, P., and J. L. Probst, A global model for present day soil CO_2 consumption by chemical erosion of continental rocks (GEM- CO_2), *Tellus, 47B*, 273-280, 1998.

Anderson, L. G., D. Dyrssen, and E. P. Jones, An assessment of the transport of atmospheric CO_2 into the Arctic Ocean, *J. Geophys. Res., 95*, 1703-1711, 1990.

Arakawa, F., Design of the UCLA general circulation model, numerical simulation of weather and climate, *Tech. Rep. 7*, Dept. of Meteorol., Univ. of Calif., Los Angeles, 1972.

Aumont, O., Etude du cycle naturel du carbone dans un modèle 3D de l'océan mondial, Ph.D. thesis, Université Pierre et Marie Curie (Paris VI), Paris, 1998.

Aumont, O., J. C. Orr, D. Jamous, P. Monfray, O. Marti, and G. Madec, A degradation approach to accelerate simulations to steady-state in a 3-D tracer transport model of the global ocean, *Clim. Dyn., 14*, 101-116, 1998.

Bluth, G. J. S., and L. R. Kump, Lithologic and climatologic controls of river chemistry, *Geochim. Cosmochim. Acta, 58*, 2341-2359, 1994.

Broecker, W. S., and T.-H. Peng, Gas exchange rates between air and the sea, *Tellus, 26*, 21-35, 1974.

Broecker, W. S., and T.-H. Peng, *Tracers in the Sea*, 690 pp., Lamont-Doherty Earth Observatory, Palisades, N.Y., 1982.

Broecker, W. S., and T.-H. Peng, Interhemispheric transport of carbon dioxide by ocean circulation, *Nature, 356*, 587-589, 1992.

Ciais, P., P. P. Tans, M. Trolier, J. W. C. White, and R. J. Francey, A large northern hemisphere terrestrial CO_2 sink indicated by the $^{13}C/^{12}C$ ratio of atmospheric CO_2, *Science, 269*, 1098-1102, 1995a.

Ciais, P., P. P. Tans, J. W. C. White, M. Trolier, R. J. Francey, J. A. Berry, D. R. Randall, P. J. Sellers, J. G. Collatz, and D. S. Schimel, Partitioning of ocean and land uptake of CO_2 as inferred by $\delta^{13}C$ measurements from the NOAA Climate Monitoring and Diagnostics Laboratory Global Air Sampling Network, *J. Geophys. Res., 100*, 5051-5070, 1995b.

Coachman, L. K., and K. Aagard, Transports through Bering Strait: Annual and interannual variability, *J. Geophys. Res., 93*, 15,535-15,539, 1988.

da Silva, A. M., C. C. Young, and S. Levitus, *Atlas of Surface Marine Data 1994*, Vol. 3: *Anomalies of Heat and Momentum Fluxes*, U.S. Dep. of Comm., Nat. Oceanic and Atmos. Admin., Nat. Environ. Satellite, Data, and Info. Serv., Washington, D.C., 1994.

Denning, A. S., I. Y. Fung, and D. Randall, Latitudinal gradient of atmospheric CO_2 due to seasonal exchange with land biota, *Nature, 376*, 240-243, 1995.

Dickson, A. G., and C. Goyet, *Handbook of Methods for the Analysis of the Various Parameters of the Carbon Dioxide System in Sea Water*, version 2, Carbon Dioxide Info. Anal. Cent., Oak Ridge Nat'l. Lab., Oak Ridge, Tenn., 1994.

Francey, R. J., P. P. Tans, C. E. Allison, I. G. Enting, J. W. C. White, and M. Troller, Changes in oceanic and terrestrial carbon uptake since 1982, *Nature, 373*, 326-330, 1995.

Gerdes, R., C. Koberle, and J. Willebrand, The influence of numerical advection schemes on the results of ocean general circulation models, *Clim. Dyn., 5*, 211-226, 1991.

Gibbs, M. T., and L. R. Kump, Global chemical erosion during the last glacial maximum and present: Sensitivity to changes in lithology and hydrology, *Paleoceanography, 9*, 529-543, 1994.

Hastenrath, S., On meridional heat transports in the world ocean, *J. Phys. Oceanogr., 12*, 922-927, 1982.

Holfort, J., K. M. Johnson, B. Schneider, G. Siedler and D. W. R. Wallace, The meridional transport of dissolved inorganic carbon in the South Atlantic Ocean, *Global Biogeochem. Cycles, 12*, 479-499, 1998.

Keeling, C. D., S. C. Piper, and M. Heimann, A three-dimensional model of atmospheric CO_2 transport based on observed winds: 4 Mean annual gradients and interannual variations, in *Aspects of Climate Variability in the Pacific and the Western Americas, Geophys. Monogr. Ser.,* vol. 55, edited by D. H. Peterson, pp. 305-363, AGU, Washington D.C., 1989.

Keeling, C. D., T. P. Whorf, M. Wahlen, and J. Van der Plicht, Interannual extremes in the rate of rise of atmospheric carbon dioxide since 1980, *Nature, 375*, 666-670, 1995.

Keeling, R. F., and T.-H. Peng, Transport of heat, CO_2 and O_2 by the Atlantic's thermohaline circulation, *Philos. Trans. R. Soc., London, Ser. B., 348*, 133-142, 1995.

Keeling, R. F., R. P. Najjar, M. L. Bender, and P. P. Tans, What atmospheric oxygen measurements can tell us about the global carbon cycle, *Global Biogeochem. Cycles*, *7*, 37-68, 1993.

Keeling, R. F., S. C. Piper, and M. Heimann, Global and hemispheric CO_2 sinks deduced from changes in atmospheric O_2 concentration, *Nature*, *381*, 218-221, 1996.

Law, R. M., et al., Variations in modeled atmospheric transport of carbon dioxide and the consequences for CO_2 inversions, *Global Biogeochem. Cycles*, *10*, 783-796, 1996.

Le Quéré, C., J. C. Orr, P. Monfray, O. Aumont, and G. Madec, Interannual variability of the oceanic sink of CO_2 from 1979 to 1997, *Global Biogeochem. Cycles*, in press, 2000.

Ludwig, W., J. L. Probst, and S. Kempe, Predicting the oceanic input of organic carbon by continental erosion, *Global Biogeochem. Cycles*, *10*, 23-42, 1996.

Madec, G., and M. Imbard, A global ocean mesh to overcome the North Pole singularity, *Clim. Dyn.*, *12*, 381-388, 1996.

Maier-Reimer, E., Geochemical cycles in an ocean general circulation model: Preindustrial tracer distributions, *Global Biogeochem. Cycles*, *7*, 645-677, 1993.

Maier-Reimer, E., and K. Hasselmann, Transport and storage of CO_2 in the ocean - An inorganic ocean circulation cycle model, *Clim. Dyn.*, *2*, 63-90, 1987.

Maier-Reimer, E., U. Mikolajewicz, and K. Hasselmann, Mean circulation of the Hamburg LSG OGCM and its sensitivity to the thermohaline surface forcing, *J. Phys. Oceanogr.*, *23*, 731-757, 1993.

Martel, F., and C. Wunsch, The North Atlantic circulation in the early 1980s-An estimate from inversion of a finite-difference model, *J. Phys. Oceanogr.*, *23*, 898-924, 1993.

Murnane, R., J. L. Sarmiento, and C. Le Quéré, Spatial distribution of air-sea CO_2 fluxes and the interhemispheric transport of carbon by the oceans, *Global Biogeochem. Cycles, 13,* 287-305, 1999.

Orr, J. C., Ocean carbon-cycle model intercomparison project (OCMIP): Phase 1 (1995-1997), *GAIM Rep. 7,* International Geosphere Biosphere Programme/Global Analysis Interpretation and Modelling Task Force Office, EOS, Univ. N.H., Durham, 1999.

Orr, J. C., E. Maier-Reimer, U. Mikolajewicz, P. Monfray, J. L. Sarmiento, J. R. Toggweiler, N. K. Taylor, J. Palmer, N. Gruber, C. L. Sabine, C. Le Quéré, R. M. Key, and J. Boutin, Estimates of anthropogenic carbon uptake from four 3-D global ocean models. *Global Biogeochem. Cycles,* in press, 2000.

Pacanowski, R., K. Dixon, and A. Rosati, The G. F. D. L. Modular Ocean Model users guide, *GFDL Ocean Group Tech. Rep.2*, Geophys. Fluid Dyn. Lab. NOAA, Princeton, N.J., 1993.

Roach, A. T., K. Aagard, C. H. Pease, S. A. Salo, T. Weingartner, V. Pavlov, and M. Kulakov, Direct measurements of transport and water properties through the Bering Strait, *J. Geophys. Res.*, *100*, 18,443-18,457, 1995.

Sarmiento, J. L., and C. Le Quéré, Oceanic carbon dioxide uptake in a model of century-scale global warming, *Science*, *274*, 1346-1350, 1996.

Sarmiento, J. L., and E. T. Sundquist, Revised budget for the oceanic uptake of anthropogenic carbon dioxide, *Nature*, *356*, 589-593, 1992.

Sarmiento, J. L., J. C. Orr, and U. Siegenthaler, A perturbation simulation of CO_2 uptake in an ocean general circulation model, *J. Geophys. Res.*, *97*, 3621-3646, 1992.

Sarmiento, J. L., R. Murnane, and C. Le Quéré, Air-Sea CO_2 transfer and the carbon budget of the North Atlantic, *Philos. Trans. R. Soc., London, Ser., B, 348*, 211-218, 1995.

Sarmiento, J. L., T. M. C. Hughes, R. J. Stouffer, and S. Manabe, Simulated response of the ocean carbon cycle to anthropogenic climate warming, *Nature*, *393*, 245-249, 1998.

Schimel, D., I. G. Enting, M. Heimann, T. M. L. Wigley, D. Raynaud, D. Alves, and U. Siegenthaler, CO_2 and the Carbon Cycle, in *Climate Change 1994*, edited by J. T. Houghton et al., pp. 35-71, Cambridge Univ. Press, New York, 1995.

Semtner, A. J., and R. M. Chervin, Ocean general circulation from a global eddy-resolving model, *J. Geophys. Res.*, *97*, 5493-5550, 1992.

Stephens, B. B., R. F. Keeling, M. Heimann, K. D. Six, R. Murnane, and K. Caldeira, Testing global ocean carbon cycle models using measurements of atmospheric O_2 and CO_2 concentrations, *Global Biogeochem. Cycles*, *12*, 213-230, 1998.

Takahashi, T., W. S. Broecker, and A. E. Bainbridge, Supplement to the alkalinity and total carbon dioxide concentration in the world ocean, in *Carbon Cycle Modelling*, SCOPE vol. 16, edited by B. Bolin, pp. 159-199, John Wiley, New York, 1981.

Takahashi, T., J. Olafsson, J. G. Goddard, D. W. Chipman, and S. C. Sutherland, Seasonal variations of CO_2 and nutrients in the high-latitude surface oceans: A comparative study, *Global Biogeochem. Cycles*, *7*, 843-878, 1993.

Takahashi, T., R. A. Feely, R. F. Weiss, R. H. Wanninkhof, D. W. Chipman, S. C. Sutherland, and T. T. Takahashi, Global air-sea flux of CO_2: An estimate based on measurements of sea-air pCO_2 difference, *Proc. Natl. Acad. Sci.*, *94*, 8292-8299, 1997.

Takahashi, T., R. H. Wanninkhof, R. A. Feely, R. F. Weiss, D. W. Chipman, N. Bates, J. Olafsson, C. Sabine, and S. C. Sutherland, Net sea-air CO_2 flux over the global oceans: An improved estimate based on the sea-air pCO_2 difference, in *Proceedings of the 2nd International Symposium, CO_2 in the Oceans*, edited by Y. Nojiri, pp. 9-14, Cent. for Global Environ. Res., Natl. Inst. for Environ. Stud., Tsukuba, 1999.

Talley, L., Meridional heat transport in the Pacific Ocean, *J. Phys. Oceanogr.*, *14*, 231-241, 1984.

Tans, P. P., I. Y. Fung, and T. Takahashi, Observational constraints on the global atmospheric CO_2 budget, *Science*, *247*, 1431-1438, 1990.

Toggweiler, J. R., K. Dixon, and K. Bryan, Simulation of radiocarbon in a coarse-resolution world ocean model, 1, Steady state prebomb distributions, *J. Geophys. Res. 94*, 8217-8242, 1989a.

Toggweiler, J. R., K. Dixon, and K. Bryan, Simulation of radiocarbon in a coarse-resolution world ocean model, 2, Distributions of bomb-produced ^{14}C, *J. Geophys. Res.*, *94*, 8243-8264, 1989b.

Trenberth, E., and A. Solomon, The global heat balance: Heat transports in the atmosphere and ocean, *Clim. Dyn.*, *10*, 107-134, 1994.

Veronis, G., The role of models in tracer studies, in *Numerical Models of Ocean Circulation*, pp. 133-146, Nat. Acad. of Sci., Washington, D. C., 1975.

Volk, T., and M. I. Hoffert, Ocean carbon pumps: Analysis of relative strengths and efficiencies in ocean-driven atmospheric CO_2 changes, in *The Carbon Cycle and Atmospheric CO_2: Natural Variations Archean to Present*, *Geophys. Monogr. Ser.*, Vol. 32, edited by E. T. Sundquist and W. S. Broecker, pp. 99-110, AGU, Washington, D.C., 1985.

Wanninkhof, R., Relationship between wind speed and gas exchange over the ocean, *J. Geophys. Res.*, *97*, 7373-7383, 1992.

Watson, A. J., P. D. Nightingale, and D. J. Cooper, Modelling atmospheric-ocean CO_2 transfer, *Philos. Trans. R. Soc. London, Ser. B, 348*, 125-132, 1995.

Weiss, R. F., Carbon dioxide in water and seawater: The solubility of a non-ideal gas, *Mar. Chem.*, *2*, 203-215, 1974.

Winguth, A. M. E., M. Heimann, K. D. Kurz, E. Maier-Reimer, U. Mikolajewicz, and J. Segschneider, El Niño-Southern Oscillation related fluctuations of the marine carbon cycle, *Global Biogeochem. Cycles*, *8*, 39-64, 1994.

O. Aumont, P. Monfray, and J. Orr, LSCE, CEA Saclay, Bât. 709, L'Orme des Merisiers, F91191 Gif-sur-Yvettte Cedex, France. (e-mail: aumont@lsce.saclay.cea.fr; monfray@cea.fr; orr@cea.fr)

E. Maier-Reimer, Max-Planck Institüt für Meteorologie, Bundestrasse 55, Hamburg, Germany. (maier-reimer@dkrz.de)

R. Murnane, Risk Prediction Initiative, Bermuda Biological Station for Research, Inc., Suite 400, 1211 Connecticut Ave, NW, Washington, DC. (rmurnane@bbsr.edu)

J. L. Sarmiento, Atmospheric and Oceanic Sciences Program, Princeton University, Sayre Hall, Forrestal Campus, P.O. Box CN710, Princeton, NJ 08544-0710. (jls@princeton.edu)

(Received January 29, 1999; revised July 27, 1999;
accepted August 9, 1999.)